JOURNAL OF ADVANCED DIELECTRICS
Vol. 4, No. 2 (2014) 1450014 (9 pages)

DOI: 10.1142/S2010135X14500143

World Scientific
www.worldscientific.com

Synthesis and characterization of lead-free ternary component BST–BCT–BZT ceramic capacitors

Venkata Sreenivas Puli*,‡, Dhiren K. Pradhan†, Brian C. Riggs*,
Shiva Adireddy*, Ram S. Katiyar† and Douglas B. Chrisey*
*Department of Physics and Engineering Physics
Tulane University, New Orleans-LA 70118, USA
†Department of Physics, University of Puerto Rico
San Juan-00936, PR, USA
‡pvsri123@gmail.com
‡vpuli@tulane.edu

Received 1 April 2014; Revised 9 May 2014; Accepted 12 May 2014; Published 10 June 2014

Polycrystalline sample of lead-free $1/3(Ba_{0.70}Sr_{0.30}TiO_3) + 1/3(Ba_{0.70}Ca_{0.30}TiO_3) + 1/3(BaZr_{0.20}Ti_{0.80}O_3)$(BST-BCT-BZT) ceramic was synthesized by solid state reaction method. Phase purity and crystal structure of as-synthesized materials was confirmed by X-ray diffraction (XRD). Temperature-dependent dielectric permittivity studies demonstrated frequency-independent behavior, indicating that the studied sample has typical diffuse phase transition behavior with partial thermal hysteresis. A ferroelectric phase transition between cubic and tetragonal phase was noticed near room temperature ($\sim$ 330 K). Bulk *P–E* hysteresis loop showed a saturation polarization of 20.4 μC/cm^2 and a coercive field of $\sim$ 12.78 kV/cm at a maximum electric field of $\sim$ 115 kV/cm. High dielectric constant ($\varepsilon \sim 5773$), low dielectric loss ($\tan\delta \sim 0.03$) were recorded at room temperature. Discharge energy density of 0.44 J/cm^3 and charge energy density of 1.40 J/cm^3 were calculated from nonlinear ferroelectric hysteresis loop at maximum electric field. Dielectric constant at variable temperatures and electric fields, ferroelectric to paraelectric phase transition and energy storage properties were thoroughly discussed.

Keywords: Crystal structure; dielectric properties; energy storage; electrical properties.

1. Introduction

Ferroelectric (piezoelectric) ceramics have been widely studied and considered as important functional materials for various electronics and microelectronics applications such as nonvolatile random access memory (NVRAM), capacitors, actuators, micro-electro-mechanical systems (MEMS) and sonar sensors. $BaTiO_3$ (BTO) was the first ABO_3 type perovskite-structured ferroelectric ceramic material studied extensively due to its high dielectric constant and higher electromechanical coupling factor.[1] Currently lead zirconate titanate (PZT) ferroelectric ceramics are most widely used in commercial piezoelectric applications due to their excellent electromechanical properties, in the proximity of the morphotropic phase boundary (MPB). Although lead-based perovskite ferroelectric materials are mostly used in solid state devices, they are facing global restrictions due to some amount of toxic lead oxide volatilization during high-temperature sintering, which in turn causes environmental pollution. Alternatively several lead-free systems were explored for multifunctional applications.[2–10] $(Na_{0.5}K_{0.5})NbO_3$ (NKN) and $(Bi_{0.5}Na_{0.5})TiO_3$ (BNT) solid solutions exhibited improved piezoelectric coefficients. However, these materials suffer poor densification due to presence of highly volatile elements like Bi, Na and K, which degraded their physical properties.[11] Bismuth potassium titanate, $(Bi_{0.5}K_{0.5}TiO_3)$, possesses good piezoelectric properties; however it is also facing restrictions due to highly volatile Bi, K elements, which in turn leads to poor densification.[12] Currently research attention considerably moved toward lead-free BTO-based solid solutions, due to their improved dielectric, ferroelectric and piezoelectric properties. These are suitable materials for capacitive energy storage applications and their physical properties can be easily customized via suitable site engineering [i.e., doping/substitution at Ba^{2+} and/or Ti^{4+}-sites with isovalent — and alio-valent (donors and acceptors) elements]. In addition to that, site engineering offers control over the electrical resistance and the ferroelectric Curie temperature.[6] It is interesting to study the influence of dielectric properties of co-substitution of Sr^{2+}, Ca^{2+} at A-site (Ba^{2+}) and Zr^{4+} in the B-site (Ti^{4+}) in BTO lattice. Due to their superior dielectric, ferroelectric, piezoelectric, pyroelectric and optical properties, BTO and its solid solutions (BST, BCT, BZT, BZT–BCT) are exclusively technically important materials in many fields including electronic industries, computer memories, video displays, microwave tunable dielectrics, phase shifters, etc.[1–8]

Ca-doped/substituted BCT solid solution ceramics have attracted much attention in materials research due to their interesting structural, dielectric, ferroelectric and piezoelectric

properties. When Ca^{2+} is substituted at Ba^{2+} in BCT lattice ($x \approx 15$ mol.%), the ferroelectric to paraelectric phase transition temperature (T_{C-T}) does not change.[13,14] Beyond the solid solubility limit ($x \approx 0.23$ mol.%) in $Ba_{1-x}Ca_xTiO_3$ lattice, tetragonal and orthorhombic phase that coexist in the BCT solid solutions have shown improved electrical properties due to the interaction of ferroelectric tetragonal and dielectric orthorhombic phases.[7,15–17] A small amount of Ca^{2+} can also occupy Ti^{4+} site in $Ba_{1-x}Ca_xTiO_3$ lattice, when Ca^{2+} occupies Ti^{4+} site in $BaTi_{1-x}Ca_xO_3$ lattice: cubic to tetragonal phase transition temperature (T_{C-T}) decreases dramatically due to internal stress (while increasing Ca^{2+} concentration).[18,19] Dissociation of oxygen can be prevented either by the substitution of lower valency ions such as Ca^{2+}/Mg^{2+} or by substitution of transition metal ions i.e., Mn^{3+}, Co^{3+} and Fe^{3+} at Ti^{4+} in BTO lattice.[20,21] When Ba^{2+} ion is replaced with Sr^{2+} ion in the BTO lattice, unit cell volume is decreased and ferroelectric to paraelectric transition temperature shifts to lower temperatures.[13,20,22,23] Interesting relaxor ferroelectric and reliable temperature-dependent dielectric properties were reported in $Ba(Zr,Ti)O_3$ bulk and thin films.[24,25] A small amount of Zr^{4+} addition to BST solid solution can significantly improve the ferroelectric and dielectric properties and reduce leakage current behavior.[26,27]

In our continuing research for materials with improved dielectric and ferroelectric properties for energy storage capacitor applications, herein we report the synthesis of ternary lead-free BST–BCT–BZT ceramics. The crystal structure, elemental analysis, dielectric and ferroelectric properties were characterized by X-ray diffraction (XRD), scanning electron microscopy (SEM) EDAX, dielectric spectroscopy and polarization measurements, respectively.

2. Experimental Method

Ternary BST–BCT–BZT ceramics with a composition of $1/3(Ba_{0.70}Sr_{0.30}TiO_3) + 1/3(Ba_{0.70}Ca_{0.30}TiO_3) + 1/3(BaZr_{0.20}Ti_{0.80}O_3) - (BST–BCT–BZT)$ were fabricated using the traditional solid-state ceramic processing route. $Ba_{0.70}Sr_{0.30}TiO_3$ (BST), $Ba_{0.70}Ca_{0.30}TiO_3$ (BCT), $BaZr_{0.20}Ti_{0.80}O_3$ (BZT) ceramics were prepared using barium carbonate ($BaCO_3$), strontium carbonate ($SrCO_3$), titanium oxide (TiO_2) and zirconium oxide (ZrO_2), (Alfa Aeasar, USA) as starting materials. Stoichiometrically weighed oxide powders were then mixed separately for 4 h by adding isopropanol on the milling media with yttrium-stabilized zirconia ball in a high-energy ball miller with intermediate interruptions for 30 min between milling. BST, BCT, BZT powders dried overnight were calcined at 1250°C for 10 h. The structure of the calcined powders were confirmed as perovskite and were re-mixed in the ratio $1/3(Ba_{0.70}Sr_{0.30}TiO_3) + 1/3(Ba_{0.70}Ca_{0.30}TiO_3) + 1/3(BaZr_{0.20}Ti_{0.80}O_3)] - (BST–BCT–BZT)$, milled again in the high-energy ball miller for 4 h using isopropanol as a milling medium with intermediate stops for 30 min. Mixed BST–BCT–BZT powders were calcined at 1250°C for 10 h and phase identified. Crystallized powder was mixed with 4% polyvinyl alcohol (PVA) as an organic binder, which increases the green strength of the pellets. Pellets were kept at 500°C for 60 min for binder removal and then sintered at 1500°C for 4 h in a carbolite furnace. The phase formation, surface morphology and compositional analysis of the sintered pellets were analyzed by XRD using $CuK_\alpha = 1.54$ Å radiation, SEM and energy-dispersive spectroscopy (EDS). Raman spectra of the sintered pellets were recorded using an ISA T64000 triple monochromator in the backscattering geometry with the help of an optical microscope equipped with an 80× objective lens which was used to focus the 514.5 nm radiation from a coherent Innova99 Ar+ laser onto the sample.

Sample with a diameter of 13 mm and a thickness of 0.3 mm was coated with silver electrode, and then the polarization versus electric field (*P–E*) hysteresis loops were characterized by Radiant technologies hysteresis loop tester (RT6000HVS-4000V) with high-voltage power supply (TREK INC., Medina, NY) under different electric fields. To measure dielectric properties, sintered discs (13 mm diameter and 2 mm thickness) were painted with silver on either side of the surfaces and were dried at 350°C for 1 h for electrode formation and moisture removal on the surface of the pellets and then ceramics pellets were poled over night at around ~50 kV/cm. The ferroelectric (*P–E*) hysteresis measurements were performed at room temperature, using a Radiant technologies hysteresis loop tester (RT6000HVS-4000V), by painting on silver electrodes on either side of the disc (13 mm diameter and 300 μm thick) with silver paint. Dielectric spectroscopy was carried on out by an automated system using a programmable temperature controller model MMR K-20 and HP4294A precision Impedance Analyzer (Agilent Technologies) over a frequency range of 1 kHz to 1 MHz, with small ac signal of 100 mV, for temperatures in the range of 100 to 480 K, at a rate of 10 K/min.

3. Results and Discussion

3.1. *Structural characterization*

Figure 1(a) shows the XRD patterns for BST, BCT, BZT sintered ceramic pellets. Crystallinity of the ceramics was characterized by XRD patterns of the ceramics in the 2θ range of 20° to 60° with a scan rate of 2° per minute. All ceramics exhibit a pure perovskite phase and no secondary phases were observed in the range investigated. Both XRD and Raman spectra confirmed tetragonal crystalline structure for ternary component ceramics. The XRD result also indicates that the ternary component BST–BCT–BZT ceramic is a single phase tetragonal perovskite structured material with space group (*P4mm*), which suggests that Ca^{2+}, Sr^{2+} entered into Ba^{2+} site and Zr^{4+} entered into Ti^{4+} site in BTO crystal lattice to form a homogeneous solid solution. It is confirmed from the XRD patterns, that the ternary component (BST–BCT–BZT)

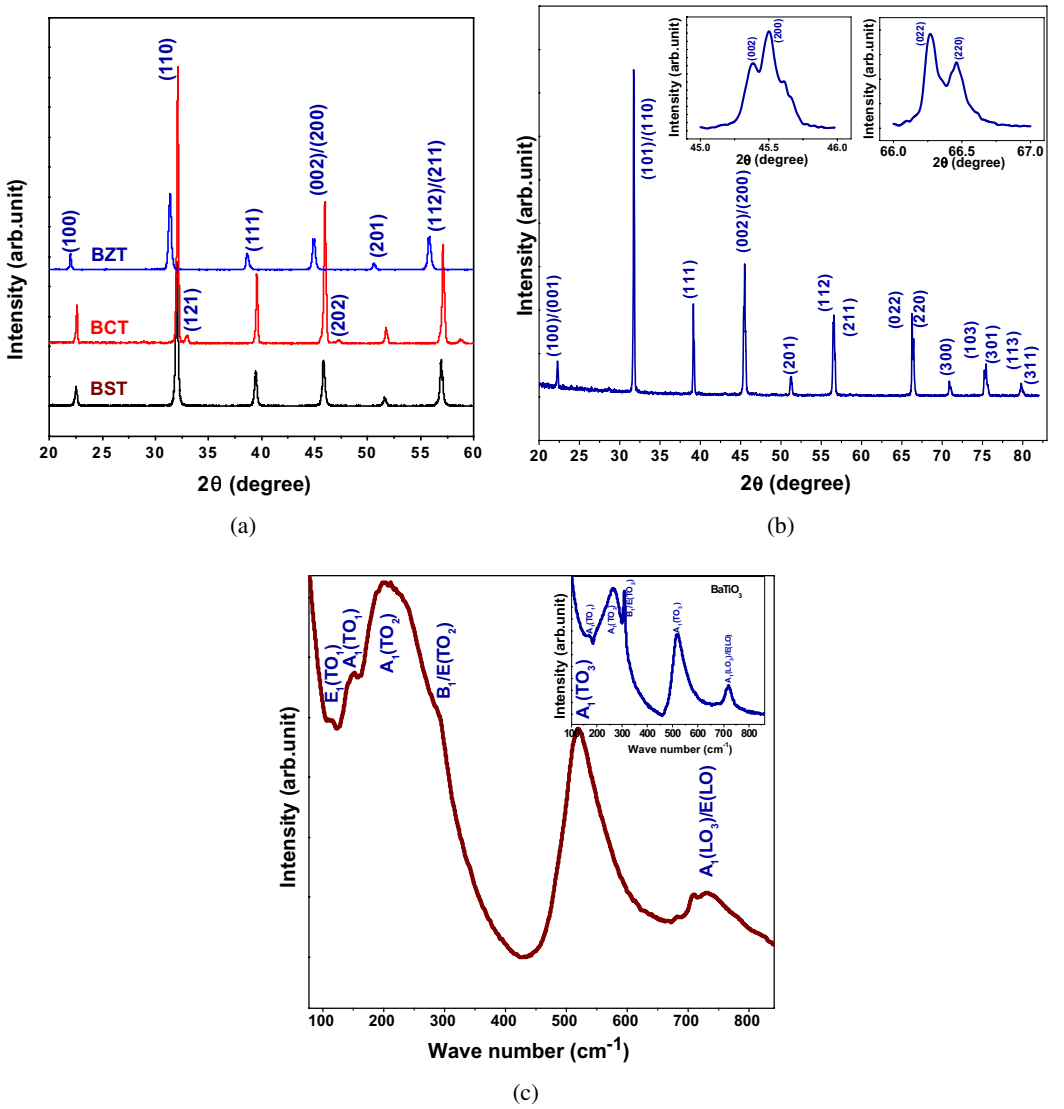

Fig. 1. (a) XRD patterns of BST, BCT, BZT ceramics at room temperature, (b) XRD patterns of BST–BCT–BZT and inset in the 2θ range of 45° to 46° and 66° to 67° of BST–BCT–BZT ceramics (The $\{2\,0\,0\}$ peak splits into (0 0 2), (2 0 0) and the $\{2\,2\,0\}$ peak splits into (0 2 2), (2 2 0) in the ternary ceramics and confirms tetragonal phase) and (c) Room temperature Raman spectra for BaTiO3 and BST–BCT–BZT ceramics.

ceramics retained phase-pure tetragonal perovskite structure at room temperature. Stable solid solutions between BST, BCT and BZT were well established. The diffraction peaks of the BST–BCT–BZT were indexed to the perovskite-type tetragonal structure with space group (*P*4*mm*) in agreement with the respective Joint Committee on Powder Diffraction Standards (JCPDS) card no 75-2119,81-2203,05-0626. The sharp and well-defined diffraction peaks indicate that this ceramic material has a good degree of crystallinity in the long range. Figure 1(b) shows the slow scan XRD patterns of BST–BCT–BZT ceramics. It is of interest to note that the tetragonal splitting of $\{2\,0\,0\}$ into (0 0 2), (2 0 0) and $\{2\,2\,0\}$ into (0 2 2), (2 2 0) in the ternary ceramics and confirms tetragonal crystal structure [inset Fig. 1(b)]. The tetragonal phase of BTO has *P*4*mm* symmetry with a c/a axis ratio close to one. The tetragonal lattice parameters for perovskite BST, BCT, BZT and ternary BST–BCT–BZT ceramics were presented in Table 1. The calculated lattice parameters $a = b = 3.98221$A, $c = 3.98835$ Å and the tetragonal distortion $(c/a) \sim 1.001$.

Local lattice distortions on an atomic scale are investigated using Raman scattering and is a powerful technique for the study of ferroelectric materials because of the close relationship between ferroelectricity and lattice dynamics.[28] In cubic phase, BTO allows 12 optical modes $(3F_{1u} + 1F_{2u})$ that are not Raman active. Room-temperature ferroelectric tetragonal BTO contain $3A1 + B1 + 4E$ Raman active phonons, which arise from three zone-center infrared active phonons (F_{1u}) and one silent mode $(E + B_1)$ comes from F_{2u}.[28]

The Raman spectra for pure BTO, ternary BST–BCT–BZT ceramics are shown in Fig. 1(c), from 100 to 800 cm^{-1} at room temperature. In brief, the room-temperature Raman

Table 1. Unit cell (lattice parameters) (a, c), tetragonal distortion (c/a), volume of unit cell for BST, BCT, BZT, ternary (BST–BCT–BZT) ceramics.

Composition	Phase	a (A)	c (A)	c/a (tetragonal distortion)	Volume (Å^3)
$Ba_{0.70}Sr_{0.30}TiO_3$	Tetragonal	3.96	3.98	1.005	62.73
$Ba_{0.70}Ca_{0.30}TiO_3$	Tetragonal	3.95	4.06	1.02	63.70
$Ba(Zr_{0.20}Ti_0.80)O_3$	Tetragonal	4.02	4.03	1.00	65.51
l/3$(Ba_{0.70}Sr_{0.30})TiO_3$– 1/3$(Ba_{0.70}Ca_{0.30})TiO_3$– 1/3$Ba(Zr_{0.20}Ti_{0.80})O_3$	Tetragonal	3.982	3.988	1.001	63.24

spectra for pure BTO ceramics have been characterized by tetragonal phase. Raman spectra corresponding to tetragonal phase were sharp modes $A_1(TO_1) \sim 170\,cm^{-1}$, $B_1/E(TO + LO) \sim 306\,cm^{-1}$ and asymmetric broader $A_1(TO_2) \sim 265\,cm^{-1}$, $A_1(TO_3) \sim 517\,cm^{-1}$, $A_1(LO)/E(LO) \sim 720\,cm^{-1}$ modes, respectively. These latter three Raman modes are also present in paraelectric cubic phase, where they are much broader and more symmetrical. The $A_1(LO)/E(LO)$ mode is extremely broad and weak in cubic phase and often considered unique to the tetragonal phase.

Tetragonal Raman modes observed for ternary BST–BCT–BZT were $E(TO_1)$, $\sim 112\,cm^{-1}$, $A_1(TO_1) \sim 150\,cm^{-1}$ [sharp mode], $A_1(TO_2) \sim 201\,cm^{-1}$ [asymmetric broad mode], $B_1/E(TO + LO) \sim 287\,cm^{-1}$, $A_1(TO_3) \sim 517\,cm^{-1}$ [asymmetric mode], $A_1(LO)/E(LO) \sim 731\,cm^{-1}$ [asymmetric broad mode], respectively. The $B_1/E(TO + LO)$ mode associated with the tetragonal-cubic phase transition, was observed at $287\,cm^{-1}$. The intensity of $B_1/E(TO + LO)$ mode is decreased due to higher amount of Sr^{2+} and Ca^{2+} content substitution at the A-site in BTO lattice in ternary BST–BCT–BZT ceramics. Orthorhombic phase in the present ceramics is also ruled out due to disappearance of Raman mode at $\sim 485\,cm^{-1}$.

The surface morphology of BST–BCT–BZT ternary ceramic system observed by SEM is displayed in Fig. 2(a). The SEM micrograph of ternary ceramic solid solution shows uniform distribution of grains throughout the surface of the sample. The grains and grain boundaries are well defined in the sample. Dense homogeneous microstructures with minimum number of voids were observed in SEM micrographs. Dense microstructure in the ternary system is attributed to effective sintering of the ceramics. The average grain size of ternary BST–BCT–BZT ceramics was 35–45 μm as shown in Fig. 2(a). Slightly enhanced grain growth is observed in this ternary ceramics which might be due to higher sintering temperature of $\sim 1500°C$. Controlled grain growth might be due to the high amount of Ba concentration when compared to Ca^{2+} and Sr^{2+}. As porosity within a ceramic reduces the ultimate breakdown strength of a material by creating a dielectric weak point, high densification is important for dielectric capacitor applications. Figure 2(a) shows a pore-free microstructure. EDAX measurement [Fig. 2(b)] shows that all the elemental peaks corresponding to ternary ceramic sample were present.

3.2. *Ferroelectric and energy storage properties*

Well-saturated P–E loop obtained in BST–BCT–BZT ternary ceramics at room temperature at different electric fields ($\sim 15\,kV/cm$–$115\,kV/cm$) are displayed in Fig. 3(a). Ternary ceramics is characterized by low remanent polarization P_r ($8.4\,\mu C/cm^2$), high maximum polarization P_{max}

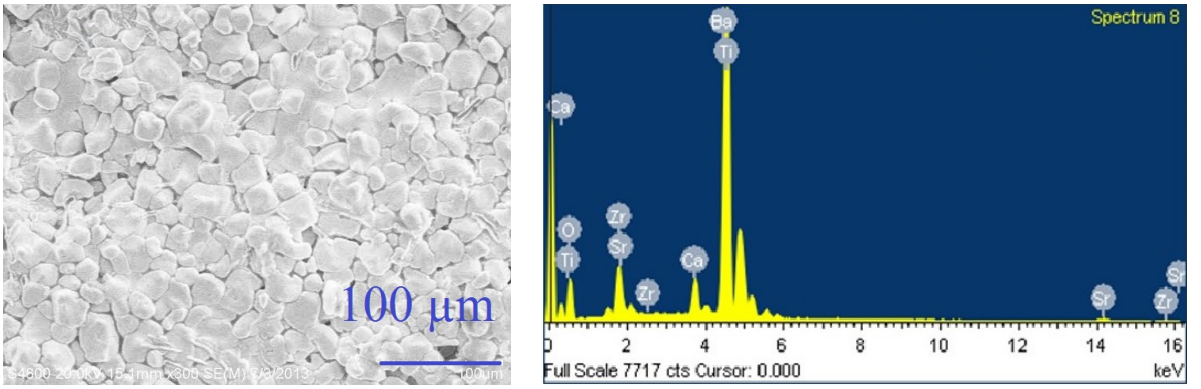

(a) (b)

Fig. 2. (a) SEM micrograph and (b) EDAX pattern of ternary (BST–BCT–BZT) ceramic sample.

($20.4\,\mu C/cm^2$) with low coercive field E_c (~ 12.78 kV/cm), while a maximum electric field of ~ 115 kV/cm. As the electric field increased from ~ 15 kV/cm to ~ 115 kV/cm, there is drastic increase in saturation polarization. The rectangular ratio (remnant polarization/maximum polarization) is 41.17%. From the hysteresis loops, it is observed that, with increasing applied electric field, remanent polarization and saturation polarization were increased with increase in coercive field. The ferroelectricity of these ternary ceramics originates from the uniform direction of Ti–O dipoles in BTO lattice.

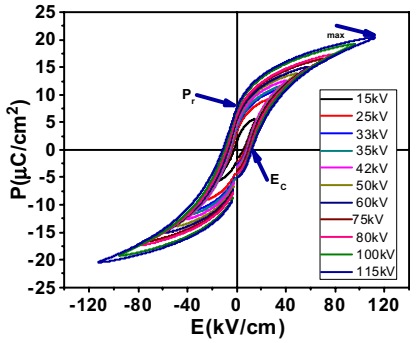

(a)

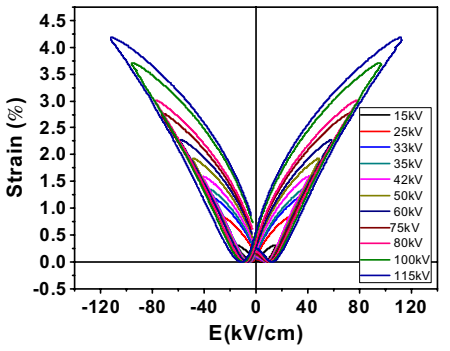

(b)

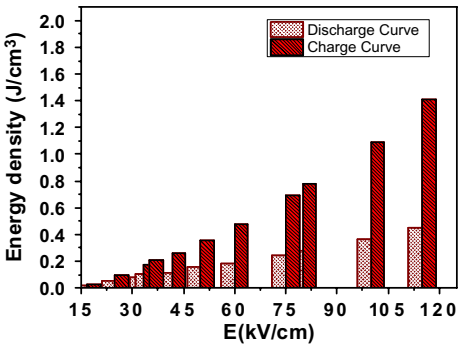

(c)

Fig. 3. (a) *P–E* loops measured at (15 kV–115 kV) in ternary BST–BCT–BZT ceramic at room temperature at 50 Hz (P_{max} — maximum polarization; P_r — remanent polarization; E_c — coercive field), (b) *S–E* loops, (c) Electric field-dependent discharge and charge energy densities of ternary (BST–BCT–BZT) ceramic sample.

The strain–electric field (*S–E*) hysteresis loops of BST–BCT–BZT ceramics obtained at room temperature (300 K) by applying an electric field of ~ 115 kV/cm is shown in Fig. 3(b). Symmetric nature of butterfly strain–electric field loops suggests the piezoelectric nature of the BST–BCT–BZT ceramics. The maximum strain percentage (S_{max}) under applied electric field (~ 115 kV/cm) is ~ 0.0416. Typical "butterfly-shaped" hysteresis loop of a sample with preset polarization can be observed in BST–BCT–BZT ceramics: after an initial low value, the strain then makes a steep increase until the maximum electric field and then decreases again to a remanent value as the field is released. The same behavior is exhibited for negative polarity electric field. This behavior is commonly connected to switching and movement of domain walls by an applied electric field. The degree of hysteresis $(\Delta x/x_{max})\% \sim 25.5\%$ was also calculated from the strain deviation during the rise and fall with the field Δx at half of the maximum field (~ 57.5 kV/cm) divided by the maximum strain x_{max} at (~ 115 kV/cm).[29] Significant reduction of the degree of hysteresis in the present ceramics might be useful for potential application as positioning actuators.

Electrical energy storage capacitors play a key role in sustainable energy program as these can enable more efficient use of energy generated from renewable sources, which will deliver very large amount of energy in a very short interval of time. Electrochemical supercapacitors offer improved power densities up to 10^6 W/kg, with moderate energy densities (0.04 to 30 W.h/kg), but their charge/discharge process is slow (require seconds or even tens of seconds) and the maximum operating temperature is typically 85°C, above this temperature these capacitors are impaired.[30,31]

Dielectric capacitors will have high power density with short discharge time ($>1\,\mu s$) when compared to batteries. Their energy density is typically much lower than electrochemical super capacitors, which is limiting their usage in device applications. Dielectric capacitors have been proposed to use in high-power application such as defibrillators, detonators, power electronics, etc due to their high electrical power output.[31] The discharge and charge energy storage densities of the ternary capacitors were calculated from the *P–E* hysteresis loops. The energy density is the integral area of the *P–E* loop (charge-curve lower branch of *P–E* curve and/or discharged curve — upper branch of *P–E* curve) and *y*-axis is given by $E_d = \int E.dP$, here E is applied electric field and P is polarization. Discharge curve energy density is the recoverable electrical energy density that is released during the discharge process from maximum electric field to zero electric field. And the stored electrical energy is the area enclosed in the hysteresis loop. Calculated energy densities for respective discharge curve and charge curves as a function of electric field is shown in Fig. 3(c) Store energy density [charge curve -0.02 to 1.40 J/cm^3] and recoverable energy density [discharge curve -0.05 to 0.44 J/cm^3] are linearly increased as the electric field increased. And the calculated energy efficiency of these ternary ceramics is $(\eta \approx J_d/J_c) \sim 31.42\%$, where J_d is discharge

curve energy density and J_c is charge curve energy density. High saturation polarization with low remnant polarization is desired for an ideal normal ferroelectric capacitor. A capacitor material with high remnant polarization is not suitable of electrical energy storage applications because the charges cannot be effectively released to the system.[30]

3.3. *Dielectric properties*

Figures 4(a) and 4(b) illustrate the temperature dependence of the dielectric constant and dielectric loss, measured at 100 Hz–1 MHz for BST–BCT–BZT ceramics sintered at 1500°C. It clearly demonstrates that dielectric constant increases slowly with increase in temperature, and a maximum dielectric constant $(\varepsilon_{max}) \sim 6143$ was observed at $(T_c) \sim 330$ K. There is significant decrease in the transition temperature of this ternary system due to complete incorporation of Sr^{2+} at Ba^{2+} site and Zr^{4+} at Ti^{4+} site in BTO however there is not much effect with Ca^{2+} substitution at Ba^{2+} site. Relatively higher dielectric permittivities at room temperature and even at transition temperature might be due to the very good densification of the ceramics. There are many factors to observe higher values of dielectric constant which include: (a) grain size; (b) change in density; (c) the grain boundary layer; (d) the release of internal stress; (f) the defect and domain wall motion.[32]

Broadening in the dielectric constant (ε) versus temperature (T) with diffuse phase transition (DPT) behavior was observed in the present ceramics and the dielectric constant decreases with further increase in temperature. There is no shift in the dielectric constant with temperature curves at all frequencies measured, which ruled out relaxor behavior for these ternary ceramics, this is also confirmed below with degree of relaxation or of diffuseness (γ). A drop in dielectric constant at high temperature and at high frequency may be noted from Fig. 4(a). Attribute is to the disappearance of spontaneous polarization as the ferroelectric tetragonal structure of ternary ceramics transforms to a paraelectric cubic phase.[2] A relatively large separation (in temperature) between the maximum of real part (dielectric constant) and imaginary (dielectric loss) part of the dielectric constant also confirms the DPT behavior.[33] It is also observed that the dielectric constant decreases with increase in frequency as expected for polar dielectric materials. The room-temperature dielectric constant and dielectric loss tangent at 100 Hz were 5792 and 0.034, respectively. Low dielectric loss (tan $\delta \sim 0.034$–0.16) values were observed throughout the measured temperature range. These low dielectric losses might be due to pore-free microstructure observed in the SEM image. Similar to dielectric constant curves, dielectric loss curves also have shown phase transition around ~ 330 K. High tan δ at low frequencies with temperature might be due to the increase in the thermally generated free carriers in the sample. The increase in tan δ at high frequencies is extrinsic in nature. It can also be seen from Fig. 4(b) that a small variation in tan δ values throughout the measured temperature occured.

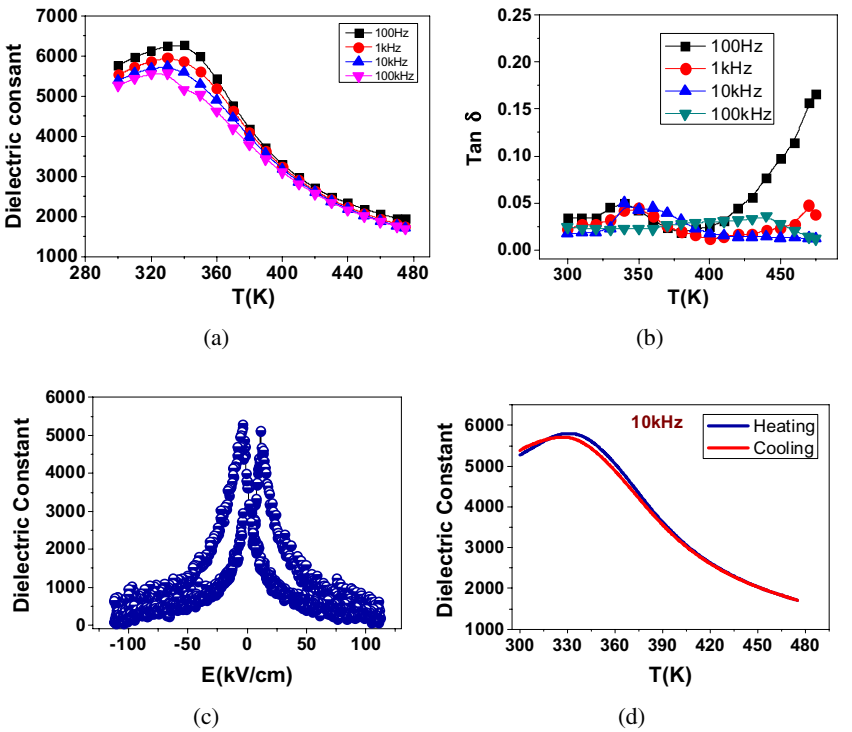

Fig. 4. (a) Temperature-dependent dielectric constant, (b) temperature-dependent dielectric loss (tan δ), (c) Electric field-dependent dielectric constant and (d) thermal hysteresis behavior for ternary (BST–BCT–BZT) ceramic sample.

However, tan δ value at 100 Hz increased above 400 K. The dc electric field dependencies on the dielectric constant at room temperature for ternary ceramics (BST–BCT–BZT) at 100 Hz are shown in Fig. 4(c). As the electric field increases, dielectric constant decreases monotonically.

3.3.1. *Dielectric thermal stability and thermal hysteresis*

Dielectric thermal stability (temperature coefficient of constant — TCP) of the ternary ceramics is calculated using the following relation (1), the lower the value of TCP, better the thermal stability.[28]

$$\text{TCP} = \frac{(\varepsilon_m - \varepsilon_{\text{ref}})}{\varepsilon_{\text{ref}}(T_m - T_{\text{ref}})}, \quad (1)$$

where, ε_m represents the maximum value of dielectric within a temperature range of interest (300 to 475 K in this experiment), T_m is the temperature corresponding to ε_m, ε_{ref} is the dielectric values at the reference temperature point T_{ref} ($T_{\text{ref}} = 475$ K in this experiment), respectively. Calculated TCP for ternary ceramics is -0.015 K (100 Hz), which is lower than BZT–BCT solid solutions (~ -0.05 K) exhibiting better thermal stability.[28]

Thermal hysteresis behavior in materials is usually considered to be an irreversible first-order phase transition phenomenon.[34] A first-order phase transition is always accompanied by the phase coexistence and the moving phase boundary interface.[35] A spontaneous transition from relaxor to normal ferroelectric state has been observed in relaxor ferroelectrics [$PbSc_{1/2}Ta_{1/2}O_3$, $PbSc_{1/2}Nb_{1/2}O_3$, $0.9PbMg_{1/3}Nb_{2/3}$–$0.1PbTiO_3$] and this transition as well posseses thermal hysteresis.[34,36,37] Partial thermal hysteresis behavior in ternary ceramics is confirmed by the measurements of the dielectric constant during heating and cooling as shown in Fig. 4(d). Very little variation in the dielectric constant was observed during heating and cooling. On heating and cooling there is no change in ferroelectric transition temperature, this might be the reason for partial thermal hysteresis behavior in present ternary ceramics with very little variation in dielectric constant. Discontinuity in the thermal hysteresis was observed at higher temperature region (400–475 K). There is not much positional change in the dielectric peak in heating and cooling cycle with respect to increase in the temperature. Complete second-order phase transition behavior (without phase coexistence) with single phase transition might be the reason for this incomplete or partial thermal hysteresis behavior in ternary ceramics.

3.3.2. *DPT behavior*

DPT behavior of the materials in dielectric spectrum is characterized by (a) dielectric constant (ε) versus temperature (T) curve broadening, (b) comparatively large separation in temperature between the maximum of the real dielectric constant and imaginary dielectric constant (loss tangent) parts of the dielectric spectrum (c) Curie–Weiss law deviation in the vicinity of T_m, and (d) frequency dispersion of dielectric properties (ε, tan δ) in the transition region thereby implying a frequency dependence of T_m.[38] Above the Curie temperature, the dielectric constant of a normal ferroelectric follows the Curie–Weiss law and is represented by Eq. (2), where ε is the dielectric constant; C, the Curie constant, T, absolute temperature and T_c, Curie temperature.

$$\frac{1}{\varepsilon} = \frac{(T - T_c)}{C}, \quad (T > T_c). \quad (2)$$

To further confirm the DPT behavior in present samples, we have plotted the reciprocal of the dielectric constant ($1/\varepsilon$) versus temperature in Fig. 5(a); the plot shown in Fig. 5(b), is fitted to a Curie–Weiss law only at temperatures far above the temperature where dielectric constant maximum occurs ($T_m = 330$ K). The reciprocal of dielectric constant ($1/\varepsilon$) starts to follow the Curie–Weiss law at temperature (T_{CWT}) = 350 K, the calculated difference between ($T_{\text{CWT}} - T_m$) = 20 K can be used as a characteristic of DPT and the extrapolated Curie–Weiss temperature (θ) = 373 K. A modified Curie–Weiss law is used to explain the dielectric behavior of

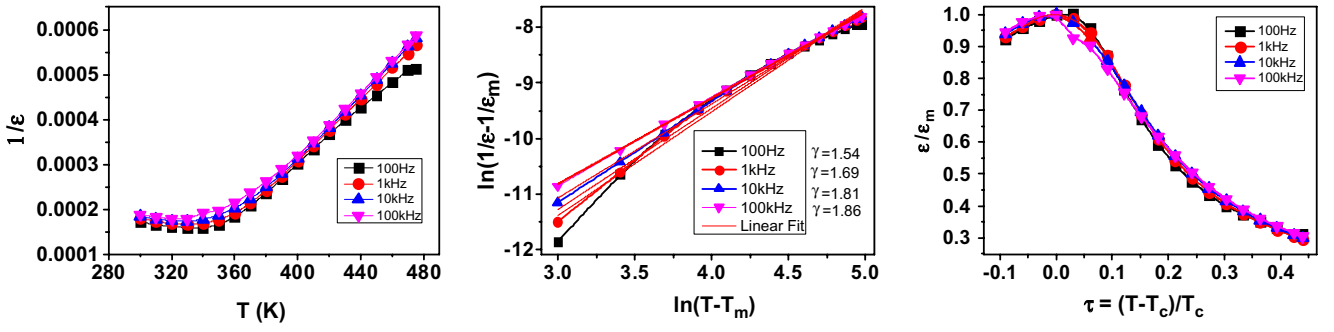

(a) (b) (c)

Fig. 5. (a) Curie–Weiss plot for the inverse of the relative dielectric permittivity–temperature ($1/\varepsilon$ versus T), (b) linear fitted log ($1/\varepsilon - 1/\varepsilon_m$) as function of log($T - T_m$) and (c) plot of reduced dielectric constant ($\varepsilon/\varepsilon_{\text{max}}$) versus reduced temperature $\tau = (T - T_c)/T_c$ in the frequency range from 100 Hz to 100 kHz.

complex ferroelectric with diffuse phase transitions,[39,40] generalized in the following Eq. (3).

$$\frac{1}{\varepsilon} - \frac{1}{\varepsilon_m} = \frac{(T - T_m)^{\gamma}}{C} \tag{3}$$

where, γ is a fitting constant; the value of γ generally lies between 1 and 2. $\gamma = 1$ represents the classical ferroelectric phase transition behavior where a normal Curie–Weiss law is followed, and $\gamma = 2$ describes diffuse (relaxor) phase transition behavior.[32,41] Figure 5(b) shows the plot of $\log\left(\frac{1}{\varepsilon} - \frac{1}{\varepsilon_m}\right)$ as a function of $\log\ (T - T_m)$ at 100 Hz–100 kHz in the temperature range of $T > T_m$, according to Eq. (3). A linear (power-law) relationship is obvious from the plot. The value of γ estimated from the slope of the graph is $\sim$(1.54, 1.69, 1.81, 1.86) indicating that the material exhibits diffuse phase transition characteristics. The values of degree of diffuseness (γ) and Curie–Weiss constant at different frequencies (100 Hz–1 MHz) were calculated using Eq. (3).

The broadening of the phase transition is better illustrated by plotting the reduced dielectric constant $(\varepsilon/\varepsilon_{\max})$ as a function of $\tau = T - T_c/T_c$ in the frequency range from 100 Hz to 100 kHz as shown in Fig. 5(c). The width of dielectric transition was characterized using the full width $\Delta\tau$ using the dielectric peaks.[36] The full width $\Delta\tau = 0.72$ of the plot has very little dispersion over a wide frequency range similar to the observation made based on relaxor materials ($\Delta\tau \sim 0.4$–0.70).[36,38]

4. Conclusion

In summary, BTO-based ternary perovskite-structured ceramic composed of $0.333[(Ba_{0.70}Sr_{0.30}TiO_3) + (Ba_{0.70}Ca_{0.30}TiO_3) + (BaZr_{0.20}Ti_{0.80}O_3)] - (BST–BCT–BZT)$ was successfully synthesized at 1500°C with promising dielectric, ferroelectric piezoelectric and energy storage properties. Tetragonal crystalline structure is confirmed using XRD and Raman spectroscopy. Well-saturated ferroelectric hysteresis loop with high dielectric constant, low dielectric loss and diffuse phase transition behavior is observed. Low coercive field and high dielectric constant at room temperature were attributed to extraordinarily soft behavior of the material. Affected by the Sr substitution at Ba-site and Zr at Ti-site, the Curie temperature of the sample was shifted to 330 K. Ca^{2+} substitution at Ba^{2+} causes a negligible change in the Curie temperature, however decrease in T_c might be attributed to partial substitution of Ca^{2+} at Ti^{4+} site in BTO lattice. Despite the excellent dielectric and ferroelectric properties, the ternary BST–BCT–BZT system exhibited a relatively low ferroelectric Curie temperature (T_c), with the energy density $\sim 0.44\ J/cm^3$ at a maximum dielectric breakdown field $\sim$(115 kV/cm). A larger electric field-induced polarization, low remanent polarization with high maximum applied electric field suggest that (BST–BCT–BZT) ternary ceramics are suitable candidate for energy storage capacitors.

Acknowledgment

This work was supported by the National Science Foundation under grant NSF-EFRI RESTOR # 1038272.

References

[1]B. Jaffe, W. R. Cook and H. Jaffe, *Piezoelectric Ceramics* (Academic Press, London, 1971).
[2]R. Thomas, V. K. Varadan, S. Komarneni and D. C. Dube, Diffuse phase transitions, electrical conduction, and low temperature dielectric properties of sol–gel derived ferroelectric barium titanate thin films, *J. Appl. Phys.* **90**(3), 1480 (2001).
[3]Y. Saito, H. Takao, T. Tani, T. Nonoyama, K. Takatori, T. Homma, T. Nagaya and M. Nakamura, Lead-free piezoceramics, *Nature* **432**, 84 (2004).
[4]P. Li, Q. Liao, Z. Zhang, Y. Zhang, Y. Huang and S. Ma, Flexible microstrain sensors based on piezoelectric ZnO microwire network structure, *Appl. Phys. Exp.* **5**, 061101 (2012).
[5]M. E. Rogers, C. M. Fancher and J. E. Blendell, Domain evolution in lead-free thin film piezoelectric ceramics, *J. Appl. Phys.* **112**, 052014 (2012).
[6]V. S. Puli, D. K. Pradhan, D. B. Chrisey, M. Tomozawa, J. F. Scott, G. L. Sharma and R. S. Katiyar, Structure, dielectric, ferroelectric and energy density properties of (1-*x*)BZT-*x*BCT ceramic capacitors for energy storage applications, *J. Mater. Sci.* **48**, 2151 (2013).
[7]V. S. Puli, D. K. Pradhan, B. C. Riggs, D. B. Chrisey and R. S. Katiyar, Investigations on structure ferroelectric piezoelectric and energy storage properties of BCT ceramics, *J. Alloys Compd.* **584**, 369 (2014).
[8]W. Li, Z. Xu, R. Chu, H. Zeng and K. Zhao, Enlarged polymorphic phase transition boundary and enhanced piezoelectricity in ternary component $0.8Ba_{1-x}Ca_xTiO_3$–$0.1BaTi_{0.8}Zr_{0.2}O_3$–$0.1BaTi_{0.9}Sn_{0.1}O_3$ ceramics, *Mater. Lett.* **110**, 80 (2013).
[9]L. Zhang, X. Wang, H. Liu and X. Yao, Structural and dielectric properties of $BaTiO_3$–$CaTiO_3$–$SrTiO_3$ ternary system ceramics, *J. Am. Ceram. Soc.* **93**(4), 1049 (2010).
[10]I. Coondoo, N. Panwar, H. Amorín, M. Alguero and A. L. Kholkin, Synthesis and characterization of lead-free 0.5Ba$(Zr_{0.2}Ti_{0.8})O_3$-0.5$(Ba_{0.7}Ca_{0.3})TiO_3$ ceramic, *J. Appl. Phys.* **113**, 214107 (2013).
[11]S. J. Zhang, R. Xia and T. R. Shrout, Modified $(K_{0.5}Na_{0.5})NbO_3$ based lead-free piezoelectrics with broad temperature usage range, *Appl. Phys. Lett.* **91**, 132913 (2007).
[12]C.-C. Huang, N. Vittayakorn and D. P. Cann, Structure and ferroelectric properties of $Bi(Zn_{1/2}Ti_{1/2})O_3$-$(Bi_{1/2}K_{1/2})TiO_3$ perovskite solid solutions, *IEEE Trans. Ultrason. Ferroelectr. Freq. Control* **56**(7), 1304 (2009).
[13]T. Mitsui and W. B. Westphal, Dielectric and X-ray studies of $Ca_xBa_{1-x}TiO_3$ and $Ca_xSr_{1-x}TiO_3$, *Phys. Rev.* **124**, 1354 (1961).
[14]M. McQuarrie and F. W. Behnke, Structural and dielectric studies in the system (Ba,Ca) (Ti,Zr)O_3, *J. Am. Ceram. Soc.* **37**, 539 (1954).
[15]V. S. Puli, D. K. Pradhan, B. C. Riggs, D. B. Chrisey and R. S. Katiyar, Structure, ferroelectric, dielectric and energy storage studies of $Ba_{0.70}Ca_{0.30}TiO_3$, $Ba(Zr_{0.20}Ti_{0.80})O_3$ ceramic capacitors, *Integr. Ferroelectr.* **157**, 1 (2014).
[16]C.-X. Li, B. Yang, S.-T. Zhang, R. Zhang, Y. Sun, J.-J. Wang, R.-X. Wang and W.-W. Cao, Phase transition, microstructure and

electrical properties of Fe doped $Ba_{0.70}Ca_{0.30}TiO_3$ lead-free piezoelectric ceramics, *Ceram. Int.* **39**, 8701 (2013).
[17]R. Buchanan, *Ceramic Materials for Electronics* (Marcel Dekker Inc, New York, 1991).
[18]L. Zhang, X. Wang, W. Yang, H. Liu and X. Yao, Structure and relaxor behavior of $BaTiO_3$-$CaTiO_3$-$SrTiO_3$ ternary system ceramics, *J. Appl. Phys.* **104**, 014104 (2008).
[19]S. Lee and C. A. Randall, A modified Vegards law for multisite occupancy of Ca in $BaTiO_3$–$CaTiO_3$ solid solutions, *Appl. Phys. Lett.* **92**, 111904 (2008).
[20]Y. Sakabe, N. Wada, T. Hiramstu and T. Tonogakiki, Dielectric properties of fine-grained BaTiO3 ceramics deoped with CaO, *Jpn. J. Appl. Phys.* **41**, 6922 (2002).
[21]V. S. Puli, I. Coondoo, N. Panwar, A. Srinivas and R. S. Katiyar, Room temperature structural, morphological, and enhanced ferroelectromagnetic properties of $xBa_{0.7}Ca_{0.3}TiO_3-(1-x)BaFe_{0.2}Ti_{0.8}O_3$ multiferroic composites, *J. Appl. Phys.* **111**(10), 102802(1) (2012).
[22]A. G. Belous, O. I. Vyunow, L. L. Kovalenko, V. Buscaglia, M. Viviani and P. Nanni, Effect of isovalent Ba-Site substitutions on the properties of $(Ba_{1-x-y}M_yY_x)TiO_3$(M = Ca, Sr, Pb) PTCR Ceramics, *Inorg. Mater.* **39**, 133 (2003).
[23]T. F. Lin, J. L. Lin and C. T. Hu, The microstructure developments and electrical properties of calcium-modified barium titanate ceramics, *J. Mater. Sci.* **26**, 491 (1991).
[24]A. Dixit, S. B. Majumder, A. Savvinov, R. S. Katiyar, R. Guo and A. S. Bhalla, Investigations on the sol–gel-derived barium zirconium titanate thin films, *Mater. Lett.* **56**, 933 (2002).
[25]T. Maiti, R. Guo and A. S. Bhalla, Structure-property phase diagram of $BaZr_xTi_{1-x}O_3$ System, *J. Am. Ceram. Soc.* **91**(6), 1769 (2008).
[26]S. Saha and S. B. Krupanidhi, Large reduction of leakage current by graded-layer La doping in $(Ba_{0.5},Sr_{0.5})TiO_3$ thin films, *Appl. Phys. Lett.* **79**, 111 (2001).
[27]G. Branch and P. W. Smith, Fast-rise-time electromagnetic shock waves in nonlinear, ceramic dielectrics, *J. Phys. D: Appl. Phys.* **29**, 2170 (1996).
[28]V. S. Puli, D. K. Pradhan, W. Pérez and R. S. Katiyar, Structure dielectric tunability thermal stability and diffuse phase transition behavior of lead-free BZT-BCT ceramic capacitors, *J. Phys. Chem. Sol.* **74**(3), 466 (2013).
[29]S. Mahajan, O. P. Thakur, D. K. Bhattacharya and K. Sreenivas, Ferroelectric relaxor behavior and impedance spectroscopy of Bi_2O_3-doped barium zirconium titanate ceramics, *J. Phys. D: Appl. Phys.* **42**, 065413 (2009).
[30]K. Yao, S. Chen, M. Rahimabady, M. S. Mirshekarloo, S. Yu, F. E. H. Tay, T. Sritharan and L. Lu, Nonlinear dielectric thin films for high-power electric storage with energy density comparable with electrochemical supercapacitors, *IEEE Trans. Ultrason. Ferroelectr. Freq. Control*, **58**(9), 1968 (2011).
[31]T. M. Correia, M. McMillen, M. K. Rokosz, P. M. Weaver, J. M. Gregg, G. Viola and M. G. Cain, A lead-free and high-energy density ceramic for energy storage applications, *J. Am. Ceram. Soc.* **96**(9), 2699 (2013).
[32]O. P. Thakur, C. Prakash and A. R. James, Effect of La substitution on the structural and dielectric properties of $BaZr_{0.1}Ti_{0.9}O_3$ ceramics, *J. Alloys Compd.* **470**, 548 (2009).
[33]V. S. Puli, R. Martinez, A. Kumar, J. F. Scott and R. S. Katiyar, A quaternary lead based Peroskite structured materials with diffuse phase transition behavior, *Mater. Res. Bull.* **46**, 2527 (2011).
[34]F. Chu, I. M. Reaney and N. Setter, Spontaneous (zero-field) relaxor–to–ferroelectric-phase transition in disordered Pb$(Sc_{1/2}Nb_{1/2})O_3$, *J. Appl. Phys.* **77**(4), 1671 (1995).
[35]S.-T. Ai, Advances in thermodynamics of ferroeletric phase transitions, in *Advances in Ferroelectrics*, ed. Dr. Aimé Peláiz-Barranco Chapter 2 (2012) In Tech., DOI:10.5772/52089, Available at http://www.intechopen.com/books/advances-in-ferroelectrics/advances-in-thermodynamics-of-ferroelectric-phase-transitions.
[36]M. Tyunina, J. Levoska, A. Sternberg and S. Leppävuori, Dielectric properties of pulsed laser deposited films of $PbMg_{1/3}Nb_{2/3}$-$PbTiO_3$ and $PbSc_{1/2}Nb_{1/2}O_3$–$PbTiO_3$ relaxor ferroelectrics, *J. Appl. Phys.* **86**(9), 5179 (1999).
[37]O. Bidault, E. Husson and A. Morell, Effects of lead vacancies on the spontaneous relaxor to ferroelectric phase transition in Pb$[(Mg_{1/3}Nb_{2/3})_{0.9}Ti_{0.1}]O_3$, *J. Appl. Phys.* **82**, 5674 (1997).
[38]A. Dixit, S. B. Majumder, A. S. Bhalla and R. S. Katiyar, Relaxor behavior in sol–gel-derived $BaZr_{0.40}Ti_{0.60}O_3$ thin films, *Appl. Phys. Lett.* **82**(16), 2679 (2003).
[39]M. Wolters and A. J. Burggraff, Relaxational polarization and diffuse phase transitions of La-substituted Pb(Zr,Ti)O_3 ceramics, *Mater. Res. Bull.* **10**, 417 (1975).
[40]G. H. Jonker, On the dielectric Curie-Weiss law an diffuse phase transition in ferroelectrics, *Mater. Res. Bull.* **18**, 301 (1983).
[41]S. K. Jo and Y. H. Han, Efiects of Sr and Ca Addition on the microstructure and the PTCR properties of Ho-doped (Ba,Sr)TiO_3, *J. Korean Phys. Soc.* **55**(2), 765 (2009).